American Mineralogist, Volume 92, pages 1760–1763, 2007

LETTER

Equations of state of $CaIrO_3$ perovskite and post-perovskite phases

TIZIANA BOFFA BALLARAN,[1,*] REIDAR G. TRØNNES,[2] AND DANIEL J. FROST[1]

[1]Bayerisches Geoinstitut, Universität Bayreuth, D-95440 Bayreuth, Germany
[2]Natural History Museum, Geology, University of Oslo, Box 1172, Blindern, N-0318 Oslo, Norway

ABSTRACT

Unit-cell lattice parameters have been measured to ~8 GPa in a diamond anvil cell for two single crystals of $CaIrO_3$: one with the perovskite (*Pbnm*) and the other with the post-perovskite (*Cmcm*) structure. The $CaIrO_3$ post-perovskite structure is more compressible than the perovskite. A third-order Birch Murnaghan equation of state has been used to fit the measured *P-V* data with the following refined parameters: V_0 = 229.463(8) Å^3, K_0 = 198(3) GPa, K' = 1.2(8); and V_0 = 226.38(1) Å^3, K_0 = 181(3) GPa, K' = 2.3(8) for $CaIrO_3$ perovskite and post-perovskite, respectively. The compressibility of the unit-cell axes of the perovskite structure is highly anisotropic with $\beta_a >> \beta_c >> \beta_b$. In contrast, the **b** axis is the most compressible in the post-perovskite structure, whereas the **a** and **c** axes have similar compressibilities (with **c** slightly less compressible than **a**) and are much stiffer. A comparison between the compressibility of $CaIrO_3$ perovskite and post-perovskite with the isostructural $MgSiO_3$ phases, reveals a similar general behavior, although in detail $CaIrO_3$ perovskite is more and the post-perovskite less anisotropic than the corresponding $MgSiO_3$ compounds.

Keywords: $CaIrO_3$ phases, high-pressure X-ray single-crystal diffraction, equation of state, perovskite and post-perovskite analogues

INTRODUCTION

$CaIrO_3$, which has the *Cmcm* space group at ambient conditions, assumes a perovskite structure with the space group *Pbnm* at pressures in the range 1–3 GPa and temperatures >1350 °C (McDaniel and Schneidler 1972; Hirose and Fujita 2005; Trønnes et al. 2006). These two phases are isostructural analogs for $MgSiO_3$ post-perovskite and perovskite, respectively, which are likely the dominant phases of the Earth's lower mantle. The phase transition of $MgSiO_3$ perovkite to post-perovskite (Murakami et al. 2004; Oganov and Ono 2004) occurs in the Earth within the D" layer, a mantle region above the core-mantle boundary with a complex seismic signature. Several experimental and numerical studies have focused on this phase transformation and on the physical properties of $MgSiO_3$ post-perovkite (Akber-Knutson et al. 2005; Caracas and Cohen 2005; Guignot et al. 2007; Iitaka et al. 2004; Mao et al. 2006; Murakami et al. 2005, 2007; Ono et al. 2006; Stackhouse et al. 2005; Tsuchiya et al. 2004a, 2004b; Wentzcovitch et al. 2004). However, the pressure and temperature conditions of the core-mantle boundary are extremely high for accurate physical property measurements; whereas ab initio calculations, which have proved to be useful in providing information beyond the experimental limits, have often reported contradictory results. The use of low-pressure analogue phases may, therefore, help to better understand the high-pressure and high-temperature behavior of the $MgSiO_3$ phases and to constrain the physico-chemical properties of the Earth's lowermost mantle. In this study, we report the equation of state of $CaIrO_3$ perovskite and post-perovskite phase determined by means of X-ray single-crystal diffraction.

EXPERIMENTAL METHOD

Sample synthesis

The sample synthesis was part of an experimental investigation of the perovskite to post-perovskite transition at 1–2.5 GPa and 1375–1525 °C, using a piston-cylinder apparatus with 0.5 inch talc-pyrex assemblies, welded Pt-capsules and W-Re-thermocouples at the Bayerisches Geoinstitut (Trønnes et al. 2006). $CaIrO_3$ perovskite crystals were synthesised at 1525 °C and 2.5 GPa using a starting material prepared from high-purity $CaCO_3$ and IrO_2 decarbonated and sintered at 900–950°C. Post-perovskite crystals were synthesized at 1435 °C and 1 GPa using a starting composition of CaO, prepared from $CaCO_3$ at 950°C, and IrO_2 where CaO was allowed to hydrate in air prior to welding into Pt capsules. In addition to post-perovskite, minor $Ca(OH)_2$ was also detected in these run products by powder X-ray diffraction.

High-pressure single-crystal X-ray diffraction

Single crystals were selected using an optical microscope according to their well-defined crystal habits, since they were too dark to base the selection on their sharp extinction. The final selection was done using a Huber single-crystal diffractometer based on the quality of Bragg reflection intensities and peak profiles.

Two $CaIrO_3$ crystals, one with the perovskite (100 × 70 × 60 μm) and the other with the post-perovskite structure (170 × 70 × 50 μm), were loaded together in a BGI-type diamond anvil cell (Allan et al. 1996) using a steel gasket T301 and a 4:1 mixture of methanol:ethanol as pressure transmitting medium. The gasket was preindented to 100 μm thickness before drilling and the gasket hole was 300 μm in

* E-mail: tiziana.boffa-ballaran@uni-bayreuth.de

diameter. Ruby spheres were used as internal diffraction pressure standards (Mao et al. 1986). The unit-cell parameters were determined at 11 different pressures up to about 7.8 GPa and at room temperature on a Huber four-circle diffractometer (non-monochromatized Mo$K\alpha$ radiation) using the eight-position centering procedure according to King and Finger (1979) and Angel et al. (2000). The centering procedure and vector-least-square refinement of the unit-cell constants were performed by SINGLE04 software according to the protocol of Ralph and Finger (1982) and Angel et al. (2000). The unit-cell data at different pressures are reported in Table 1.

Results

The variation of the unit-cell volume as a function of pressure is shown in Figure 1 for both crystals. No discontinuity has been observed up to 7.8 GPa. A further increase in pressure was not possible due to a failure of the gasket; data were instead collected on decompression. The data point collected in decompression at 5.26 GPa for the perovskite sample resulted from reflections with quite large profiles (likely due to the fact that the crystal was bridged between the diamonds). For this reason the data collected in decompression were not considered during the equation of state fitting procedure. A third-order Birch-Murnaghan equation of state (BM3 EoS) was used to fit the *P*-*V* data (Eosfit52 program; Angel 2002). The resulting EoS parameters are reported in Table 2. The first pressure derivative, K', of the bulk modulus, K_0, is smaller than 4 for both samples. These values are in excellent agreement with those obtained from weighted fits of the "normalized stress" $F_E = P/3f_E(1 + 2f_E)^{5/2}$ – finite strain $f_E = [(V_0/V)^{2/3} - 1]/2$ plot (Angel 2000) shown in Figure 2. The axial compressibilities of both samples are strongly anisotropic (Figs. 3 and 4) as shown by the BM3 EoS parameters obtained for the unit-cell axes (Table 2). The values of the "linear"-K_0 obtained from the BM3 EoS fits of the unit-cell axes are one third of the inverse of the linear compressibility $\beta_0 = \frac{1}{l_0}\left(\frac{\delta l}{\delta P}\right)_{P=0}$ (Angel 2000) also reported in Table 2.

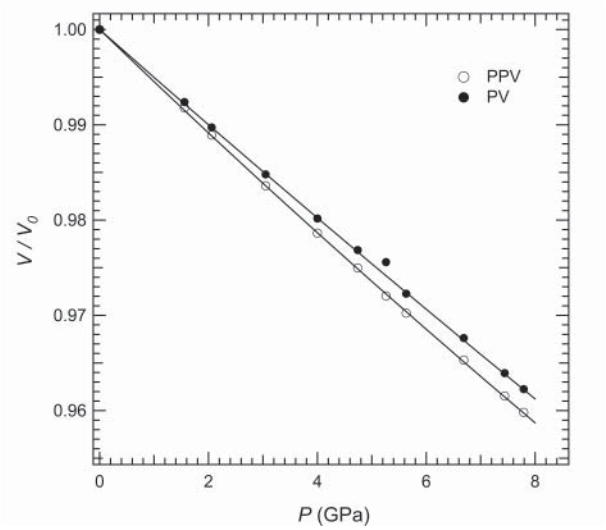

Figure 1. Unit-cell volume variation of $CaIrO_3$ perovskite (filled circles) and post-perovskite (open circles) crystals as a function of pressure. Solid lines are third-order Birch-Murnaghan EoS fits through the data. Uncertainties are smaller than the symbols used except for the data point at 5.26 GPa collected for the perovskite sample, whose reflection profiles were quite broad and which falls outside the EoS fit.

Discussion

$CaIrO_3$ post-perovskite is more compressible than the perovskite polymorph, mainly as a result of the major difference in compressibility of the **b** axis between the two structures (Table 2, Figs. 3–4). The same applies to the isostructural $MgSiO_3$

Table 1. Lattice parameters collected at different pressures for $CaIrO_3$ perovskite and post-perovskite crystals

P (GPa)	*a* (Å)	*b* (Å)	*c* (Å)	*V* (Å)
		Perovskite (*Pbnm*)		
0.00010(1)	5.34765(10)	5.59186(9)	7.6735(2)	229.463(8)
1.56(5)	5.32906(13)	5.58355(12)	7.6531(3)	227.718(12)
2.06(5)	5.32251(9)	5.58091(12)	7.64550(12)	227.105(10)
3.05(5)	5.31005(11)	5.57602(11)	7.6320(3)	225.976(10)
4.00(5)	5.29799(11)	5.57157(11)	7.6194(3)	224.911(11)
4.74(5)	5.28937(11)	5.56848(10)	7.6103(2)	224.152(10)
5.63(5)	5.27702(9)	5.56466(10)	7.5976(2)	223.100(9)
6.69(5)	5.26435(10)	5.56066(12)	7.5848(3)	222.032(11)
7.44(5)	5.25429(11)	5.55758(12)	7.5746(3)	221.188(10)
7.79(5)	5.24959(8)	5.55629(9)	7.5699(2)	220.801(8)
5.26(5)*	5.2846(8)	5.5684(9)	7.607(2)	223.86(8)
		Post-perovskite (*Cmcm*)		
0.00010(1)	3.14541(12)	9.8618(3)	7.29788(11)	226.376(12)
1.56(5)	3.13844(10)	9.8224(3)	7.28301(9)	224.513(10)
2.06(5)	3.13613(9)	9.8083(2)	7.27784(8)	223.868(10)
3.05(5)	3.13176(10)	9.7822(3)	7.26821(9)	222.665(10)
4.00(5)	3.12768(12)	9.7573(4)	7.25933(11)	221.539(12)
4.74(5)	3.12487(17)	9.7383(5)	7.25286(17)	220.711(17)
5.63(5)	3.12079(9)	9.7150(2)	7.24434(8)	219.638(9)
6.69(5)	3.11669(9)	9.6900(2)	7.23571(8)	218.524(8)
7.44(5)	3.1136(8)	9.6706(2)	7.22909(7)	217.670(7)
7.79(5)	3.1121(2)	9.6620(6)	7.2259(2)	217.28(2)
5.26(5)*	3.12238(8)	9.7241(2)	7.24736(7)	220.047(8)

Note: Standard deviations are in parentheses.
* Data point measured in decompression.

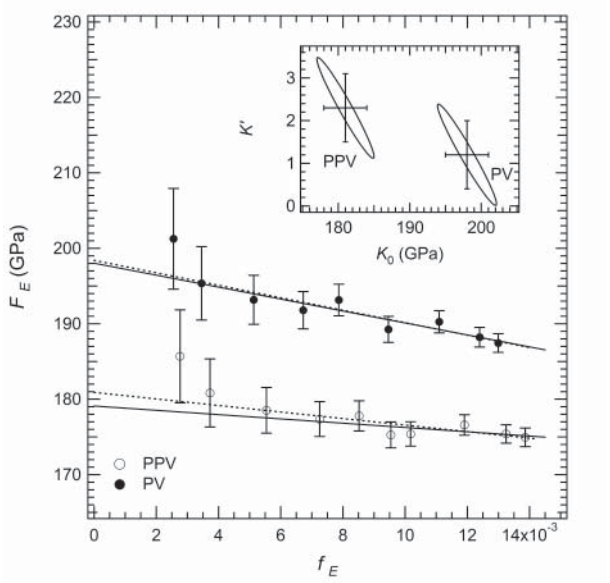

Figure 2. F_E-f_E plot based on the Birch-Murnaghan EoS for $CaIrO_3$ perovskite (filled circles) and post-perovskite (open circles) crystals. The values of V_0 used to calculate the finite strain are those measured at room pressure. Dotted lines are weighted fits through all the data having the following equations: $F_E = 198(3) - 825(244)f_E$ and $F_E = 181(2) - 433(214)f_E$ for $CaIrO_3$ perovskite and post-perovskite, respectively. Solid lines are weighted fits through the data collected at $P > 4$ GPa. Confidence ellipses in K_0 and K' equivalent of 1σ for a normal distribution of a single variable for the fits of the BM3 EoS to the *P*-*V* data of $CaIrO_3$ perovskite and post-perovskite are shown in the inserted graph.

TABLE 2. BM3 EoS parameters fitted to the $CaIrO_3$ perovskite and post-perovskite compressibility data

	Perovskite (*Pbnm*)	Post–perovskite (*Cmcm*)
a_0 (Å)	5.3477(1)	3.1454(1)
$K_0(a)$ (GPa)	146(2)	228(5)
K'	−1.0(5)	4(1)
β_{0a} (GPa^{-1})	0.00228	0.00146
b_0 (Å)	5.5919(1)	9.8619(3)
$K_0(b)$ (GPa)	322(7)	124(2)
K'	26(3)	0.9(5)
β_{0b} (GPa^{-1})	0.00104	0.00269
c_0 (Å)	7.6735(2)	7.2979(1)
$K_0(c)$ (GPa)	187(3)	243(4)
K'	1.2(8)	5(1)
β_{0c} (GPa^{-1})	0.00178	0.00137
V_0 ($Å^3$)	229.463(8)	226.38(1)
K_0 (GPa)	198(3)	181(3)
K'	1.2(8)	2.3(8)

Note: Standard deviations are in parentheses.

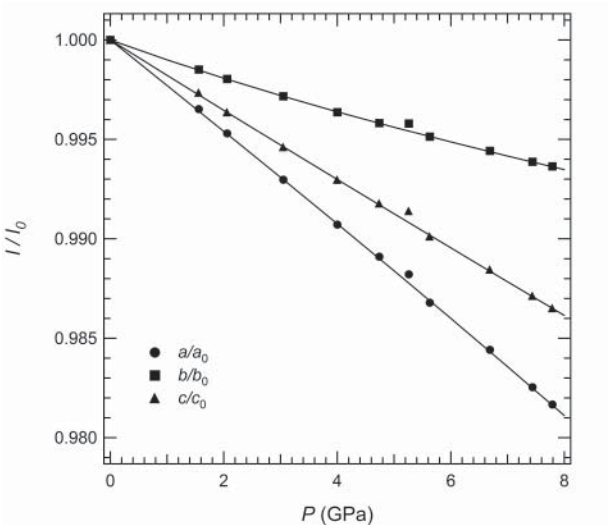

FIGURE 3. Axial compressibility of $CaIrO_3$ perovskite phase. Filled circles: **a** axis; filled squares: **b** axis; and filled triangles: **c** axis. Solid curves are BM3 EoS fits through the data. Uncertainties are smaller than the symbols used except for the data point at 5.26 GPa (see text).

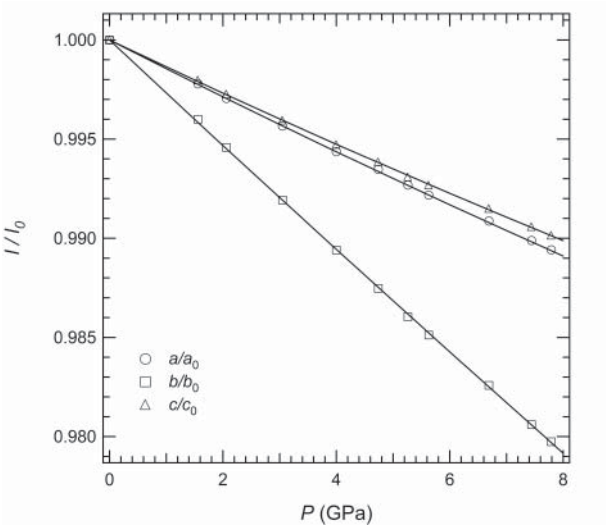

FIGURE 4. Axial compressibility of $CaIrO_3$ post-perovskite phase. Open circles: **a** axis; open squares: **b** axis; and open triangles: **c** axis. Solid curves are BM3 EoS fits through the data. Uncertainties are smaller than the symbols used.

phases, as indicated by experimental and computational studies (Akber-Knutson et al. 2005; Caracas and Cohen 2005; Guignot et al. 2007; Ono et al. 2006; Shieh et al. 2006). The values of K' reported in Table 2 for the two phases appear to be the same given the uncertainties, however a careful analysis of the *F-f* plot (Fig. 2) shows that the *P-V* data are indeed consistent with post-perovskite becoming more incompressible with pressure relative to perovskite. In fact, linear weighted fits of the high-pressure *F-f* data alone (for P > 4 GPa) do not differ significantly from those obtained considering the entire pressure range and give K_0 and K' values in excellent agreement with those obtained from the BM3 EoS fits. This result supports theoretical calculations which indicate that the K' of $MgSiO_3$ post-perovskite is slightly larger than that of $MgSiO_3$ perovskite (Akber-Knutson et al. 2005; Caracas and Cohen 2005). Such a conclusion had not been supported to date by experimental results, which, given the high pressures required, have always reported K' for $MgSiO_3$ perovskite and post perovskite fixed to the value of 4 (Fiquet et al. 2000; Andrault el al. 2001; Ono et al. 2006; Shieh et al. 2006; Guignot et al. 2007).

The axial compressibility ratios β_{0a}:β_{0b}:β_{0c} are 1:0.46:0.78 and 0.54:1:0.51 for $CaIrO_3$ perovskite and post-perovskite, respectively. The axial compressibility scheme of $CaIrO_3$ perovskite is similar, although more pronounced, to that reported for $MgSiO_3$ perovskite (Ross and Hazen 1990; Fiquet et al. 2000; Wentzcovitch et al. 1998; Vanpeteghem et al. 2006), with the **b** axis much less compressible than the other two unit-cell directions. However, the compressibility of the **a** and **c** axes is almost the same in $MgSiO_3$ perovskite. In contrast, although the compressibility scheme of $CaIrO_3$ and $MgSiO_3$ post-perovskite are also similar, it appears that the anisotropy of $MgSiO_3$ post-perovskite is more pronounced if the room pressure compressibility values are considered (Guignot et al. 2007). However, the axial compressibility ratios at 136 GPa and 0 K (Stackhouse et al. 2005) in the stability field of $MgSiO_3$ post-perovskite are similar to those obtained in this study for its low-pressure analogue. The major difference between the compressibility schemes of perovskite and post-perovskite is shown by the **b** axis, which is the direction along which the three-dimensional octahedral framework of perovskite is broken to give rise to the octahedral layers of the post-perovskite structure. The increase of compressibility along the **b** axis of post-perovskite with respect to perovskite seems to account for the smaller bulk modulus value obtained for the former.

Our high-pressure experimental results on the elasticity of the $CaIrO_3$ polymorphs are broadly consistent with the density functional theory (DFT) modeling of Stølen and Trønnes (2007). The DFT-study gives zero pressure crystallographic axes of both polymorphs that are slightly shorter (average 98.9%) than those measured experimentally, with the unit-cell volume difference of 2.7% for perovskite and 3% for post-perovskite, which is on the

order of the standard precision of the DFT calculations. Whereas the relative axial compressibilities from DFT and experiments are in close agreement, the DFT-model predicts slightly more compressible axes for both polymorphs, except for the **b**-axis in perovskite, which is slightly less compressible.

The combined experimental and computational results indicate that the $CaIrO_3$ system is a useful low-pressure analogue for the high-pressure perovskite to post-perovskite transition in $MgSiO_3$-rich materials in the lowermost mantle. Because the K' is larger for the most compressible phase, post-perovskite, an extrapolation beyond 15–20 GPa of the low pressure K_0 values obtained for the range 0–8 GPa will make $CaIrO_3$ perovskite more compressible than the corresponding post-perovskite. An equivalent change will occur for a similar extrapolation for the $MgSiO_3$ analogs, because the K' is larger for the most compressible post-perovskite phase also in this system (Sheih et al. 2006).

ACKNOWLEDGMENTS

The high-pressure syntheses were performed at the Bayerisches Geoinstitut under the EU "Research Infrastructures: Transnational Access" Programme [Contract No. 505320 (RITA)—High Pressure]. S. Stølen provided Ir and IrO_2 and assisted with the starting material preparation, and G. Gudfinnsson, S. Keshav, and C. McCammon helped with the piston-cylinder experiments. Two anonymous reviewers are thanked for their helpful comments.

REFERENCES CITED

Akber-Knutson, S., Steinle-Neumann, G., and Asimow, P.D. (2005) Effect of Al on the sharpness of the $MgSiO_3$ perovskite to post-perovskite phase transition. Geophysical Research Letters, 32, L14303, DOI: 10.1029/2005GL023192.

Allan, D.R., Miletich, R., and Angel, R.J. (1996) A diamond-anvil cell for single-crystal X-Ray diffraction studies to pressures in excess of 10 GPa. Review of Scientific Instruments, 67, 840–842.

Andrault, D., Bolfan-Casanova, N., and Guignot, N. (2001) Equation of state of lower mantle (Al,Fe)-$MgSiO_3$ perovskite. Earth and Planetary Science Letters, 193, 501–508.

Angel, R.J. (2000) Equation of state. In R.M. Hazen and R.T. Downs, Eds., High-Temperature and High-Pressure Crystal Chemistry, 41, p. 35–59. Reviews in Mineralogy and Geochemistry, Mineralogical Society of America, Chantilly, Virginia.

——— (2002) EOS-FIT5.2. Computer program. Crystallography Laboratory, Department of Geological Sciences, Virginia Tech, Blacksburg.

Angel, R.J., Downs, R.T., and Finger, L.W. (2000) High-temperature-high-pressure diffractometry. In R.M. Hazen and R.T. Downs, Eds., High-Temperature and High-Pressure Crystal Chemistry, 41, p. 559–596. Reviews in Mineralogy, Mineralogical Society of America, Chantilly, Virginia.

Caracas, R. and Cohen, R.E. (2005) Effect of chemistry on the stability and elasticity of the perovskite and post-perovskite phases in the $MgSiO_3$-$FeSiO_3$-Al_2O_3 system and implications for the lowermost mantle. Geophysical Research Letters, 32, L16310, DOI: 10.1029/2005GL023164.

Fiquet, G., Dewaele, A., Andrault, D., Kunz, M., and Le Bihan, L. (2000) Thermoelastic properties and crystal structure of $MgSiO_3$ perovskite at lower mantle pressure and temperature conditions. Geophysical Research Letters, 27, 21–24.

Guignot, N., Andrault, D., Morard, G., Bolfan-Casanova, N., and Mezouar, M. (2007) Thermoelastic properties of post-perovskite phase $MgSiO_3$ determined experimentally at core-matle boundary *P-T* conditions. Earth and Planetary Science Letters, 256, 162–168.

Hirose, K. and Fujita, Y. (2005) Clapeyron slope of the post-perovskite phase transition in $CaIrO_3$. Geophysical Research Letters, 32, L13313, DOI: 10.1029/2005GL023219.

Iitaka, T., Hirose, K., Kawamura, K., and Murakami, M. (2004) The elasticity of the $MgSiO_3$ post-perovskite phase in the Earth's lowermost mantle. Nature, 430, 442–444.

King, H.E. and Finger, L.W. (1979) Diffracted beam crystal centering and its application to high-pressure crystallography. Journal of Applied Crystallography, 12, 374–378.

Mao, H.-K., Xu, J., and Bell, P.M. (1986) Calibration of the ruby pressure gauge to 800 kbar under quasi-hydrostatic conditions. Journal of Geophysical Research, 91, 4673–4676.

Mao, W. L., Mao, H.-K., Prakapenka, V.B., Shu, J.F., and Hemley, R.J. (2006) The effect of pressure on the structure and volume of ferromagnesian post-perovkiste. Geophysical Research Letters, 33, L12S02, DOI: 10.1029/2006GL25770.

McDaniel, C.L. and Schneidler, S.J. (1972) Phase relations in the CaO-IrO_2-Ir system in air. Journal of Solid State Chemistry, 4, 275–280.

Murakami, M., Hirose, K., Kawamura, K., Sata, N., and Ohishi, Y. (2004) Post-perovskite phase transition in $MgSiO_3$. Science, 304, 855–858.

Murakami, M., Hirose, K., Sata, N., and Ohishi, Y. (2005) Post-perovskite phase transition and mineral chemistry in the pyrolitic lower mantle. Geophysical Research Letters, 32, L03304, DOI: 10.1029/2004GL020648.

Murakami, M., Sinogeikin, S.V., Bass, J.D., Sata, N., Ohishi, Y., and Hirose, K. (2007) Sound velocity of $MgSiO_3$ post-perovskite phase: A constraint on the D" discontinuity. Earth and Planetary Science Letters, 259, 8–23, DOI: 10.1016/j.epsl.2007.04.015.

Oganov, A.R. and Ono, S. (2004) Theoretical and experimental evidence for a post-perovskite phase of $MgSiO_3$ in Earth's D" layer. Nature, 430, 445–448.

Ono, S., Kikegawa, T., and Ohishi, Y. (2006) Equation of state of $CaIrO_3$-type $MgSiO_3$ up to 144 GPa. American Mineralogist, 91, 475–478.

Ralph, R.L. and Finger, L.W. (1982) A computer program for refinement of crystal orientation matrix and lattice constants from diffractometer data with lattice symmetry constraints. Journal of Applied Crystallography, 15, 537–539.

Ross, N.L. and Hazen, R.M. (1990) High-pressure crystal chemistry of $MgSiO_3$ perovskite. Physics and Chemistry of Minerals, 17, 228–237.

Shieh, S.R., Duffy, T.S., Kubo, A., Prakapenka, V.B., Sata, N., Hirose, K., and Ohishi, Y. (2006) Equation of state of the post-perovskite phase synthesized from a natural (Mg,Fe)SiO_3 orthopyroxene. Proceedings of the National Academy of Science, 103, 3039–3043.

Stackhouse, S., Brodholt, J.P., Wookey, J., Kendall, J.-M., and Price, G.D. (2005) The effect of temperature on the seismic anisotropy of the perovskite and post-perovkiste polymorphs of $MgSiO_3$. Earth and Planetary Science Letters, 230, 1–110.

Stølen, S. and Trønnes, R.G. (2007) The perovskite to post-perovskite transition in $CaIrO_3$: Clapeyron slope and changes in bulk and shear moduli by density functional theory. Physics of Earth and Planetary Interiors, in press, DOI: 10.1016/j.pepi.2007.05.009.

Trønnes, R.G., Frost, D.J., Boffa Ballaran, T., and Stølen, S. (2006) The perovskite to post-perovskite transition in $CaIrO_3$. American Geophysical Union Fall Meeting, MR11A97.

Tsuchiya, J., Tsuchiya, T., and Wentzcovitch, R.M. (2004a) Vibrational and thermodynamic properties of $MgSiO_3$ post-perovskite. Journal of Geophysical Research, 110, B02204.

Tsuchiya, T., Tsuchiya, J., Umemoto, K., and Wentzcovitch, R.M. (2004b) Elasticity of post-perovskite $MgSiO_3$. Geophysical Research Letters, 31, L14603, DOI: 10.1029/2004GL020278.

Vanpeteghem, C.B., Zhao, J., Angel, R.J., Ross, N.L., and Bolfan-Casanova, N. (2006) Crystal structure and equation of state of $MgSiO_3$ perovskite. Geophysical Research Letters, 33, L03306, DOI: 10.1029/2005GL024955.

Wentzcovitch, R.M., Karki, B.B., Karato, S., and Da Silva, C.R.S. (1998) High-pressure elastic anisotropy of $MgSiO_3$ perovskite and geophysical implications. Earth and Planetary Science Letters, 165, 371–378.

Wentzcovitch, R.M., Karki, B.B., Cococcioni, M., and de Gironcoli, S. (2004) Thermoelastic properties of $MgSiO_3$-perovskite: Insights on the nature of the Earth's lower mantle. Physical Review Letters, 92, 018501.

MANUSCRIPT RECEIVED JUNE 13, 2007
MANUSCRIPT ACCEPTED JUNE 26, 2007
MANUSCRIPT HANDLED BY BRYAN CHAKOUMAKOS

NOTE ADDED IN PROOF

A recent report of a high-pressure powder diffraction study of $CaIrO_3$ post-perovskite (Martin et al. 2007, *American Mineralogist*, vol. 92, p. 1048–1053) presents second-order Birch-Murnaghan EoS parameters (K' fixed to 4), which are in general agreement with the results obtained in this study for the same phase.